1996A&A...308..713F

Astron. Astrophys. 308, 713–722 (1996)

ASTRONOMY AND ASTROPHYSICS

Large-field optical polarimetry of NGC 891, 5907 and 7331

Selecting the intrinsic polarising mechanism

C. Fendt[1,2], R. Beck[3], H. Lesch[2,3], and N. Neininger[3,4]

[1] Lund Observatory, Box 43, S-22100 Lund, Sweden
[2] Landessternwarte Königstuhl, D-69117 Heidelberg, Germany
[3] Max-Planck-Institut für Radioastronomie, Auf dem Hügel 69, D-53121 Bonn, Germany
[4] IRAM, 300, rue de la Piscine, F-38406 St. Martin d'Heres, France

Received 20 April 1995 / Accepted 13 August 1995

Abstract. Large-scale images in linear optical polarisation of three edge-on spiral galaxies (NGC 891, 5907, 7331) are presented.

The dominant orientation of the polarisation pattern in all observed galaxies is perpendicular to the major axis and seems to be given by anisotropic scattering effects. However, we also found evidence for polarisation due to the Davis-Greenstein mechanism. In a region located towards the central part of NGC 891 within the dust lane, the derived orientation of the magnetic field is perpendicular to the major axis. In NGC 7331, the polarisation along the western dust lane indicates a toroidal field. No other indication for disk-parallel (toroidal) magnetic fields in the observed galaxies could be found.

Key words: polarization – galaxies: magnetic field – galaxies: ISM – galaxies: individual: NGC 891, 5907, 7331

1. Introduction

For decades optical polarisation measurements have been used as indicators for large-scale magnetic fields in galaxies. Some milestones were the detection of interstellar polarisation of starlight (Hiltner & Hall 1949), an explanation of this polarisation by selective extinction of magnetically aligned dust grains (Davis & Greenstein 1951), and the discovery of optical polarisation in galaxies (Elvius 1956; Appenzeller 1967) as well as a polarisation map of the whole sky (Mathewson & Ford 1970).

The basic physical mechanism producing linear optical polarisation is scattering of light by dust grains. The observed polarisation therefore depends on the intrinsic light distribution, the dust distribution, the grain size, and the chemical composition of the dust grains. In the optical wavelength regime, two contributions have to be taken into account for the interpretation of observed polarisation: (1) Anisotropic scattering by spherical particles and (2) the Davis-Greenstein mechanism (hereafter DGM), the effect of selective extinction by elongated dust grains aligned by a magnetic field (Davis & Greenstein 1951; Spitzer 1978).

Both processes have different efficiencies and different dependences on wavelength and scattering angle. In principle, these parameters could be used to estimate their contribution to the observed polarisation.

Unfortunately, from the observational point of view, the DGM possesses a kind of "self-obscuring" property: The most likely sites for the DGM, i.e. dust clouds or dust disks in galaxies, also undergo high interstellar extinction. Due to the very low intensity in these regions, a detection of the already weak DGM is extremely difficult.

While optical polarisation measurements of galaxies continue (e.g. Bingham et al. 1976; King 1986; Scarrott et al. 1983, 1990, 1993), it remains unclear to what extent anisotropic scattering may rule out selective extinction effects.

A realistic quantitative analysis can only be made using explicit scattering model calculations for each galaxy. This, however, requires observational data of intrinsic properties of the distribution of light, dust and magnetic field. Otherwise, the set of free parameters may exceed the fixed quantities. Only in case of certain configurations of the polarisation pattern, these two polarising mechanisms may be distinguished.

Furthermore, observations in different wavelengths (see e.g. Scarrott et al. 1990) would support the distinction, although we believe that for this purpose, the optical spectral range is too small.

With its improved observational technology, radio polarisation now provides the best, because is direct, indicator for interstellar magnetic fields (Beck 1991, 1993; Wielebinski & Krause 1993; Kronberg 1994). However, in some examples the interpretation of the radio data is not straightforward due to Faraday rotation and de-polarisation by ionised interstellar and coronal matter (Beck 1993). In these cases, optical polarisation

Send offprint requests to: C. Fendt (Lund Observatory)

© European Southern Observatory • Provided by the NASA Astrophysics Data System

1996A&A...308..713F

measurements may provide a test for the radio data, if both polarising mechanisms are due to the same magnetic fields. The orientation of the optical E-vectors would indicate the amount of Faraday rotation of the intrinsic B-vectors in the radio range. Additionally, they allow for estimates of the gas and dust distribution in the observed galaxies.

In this paper, we present linear optical polarisation observations of NGC 891, 5907, 7331. These are nearby, edge-on spiral galaxies, showing dark dust lanes which, together with possible magnetic fields, provide the conditions where the DGM may work and might be observable.

Edge-on galaxies were chosen in order to allow a better distinction between the DGM in a toroidal field and anisotropic scattering of light from the central region. In face-on galaxies both anisotropic scattering and the DGM would similarly produce a circular pattern of the polarisation vectors. In edge-on galaxies, polarisation vectors produced by the DGM are expected to be perpendicular to the vectors caused by anisotropic scattering.

Furthermore, we chose a sample of some of the most extensively observed spiral galaxies. Dumke et al. (1995) observed NGC 891, 5907 and 7331 in radio continuum at λ 2.8cm with a linear resolution of 69″. In this wavelength range Faraday effects are negligible and the intrinsic magnetic field orientation can directly be deduced from the observed polarisation angle. Dumke et al. obtained the following results: NGC 891 shows emission up to large distances from the disk (3-5 kpc). The magnetic field in this radio halo is preferentially parallel to the disk. NGC 5907 and NGC 7331 have almost no radio halo; the extension of the emission is less than 1 kpc. No significant polarisation was detected in NGC 5907. The field structure in NGC 7331 is mainly parallel to the disk.

Small-field optical polarisation maps (NGC 5907, Scarrott et al. 1990; NGC 7331, Elvius 1956; King 1986) allow tests of our large-field maps, while Hα imaging (NGC 891, Dettmar 1990; Rand et al. 1990) and model calculations (Jura 1982; Matsumara & Seki 1989; Kylafis & Bahcall 1987) give hints to the gas and dust distribution.

2. Instrument and observations

Our observations were performed at the 1.23m telescope of the DSAZ[1] (Deutsch-Spanisches Astronomisches Zentrum), Calar Alto, Spain, using the CCD polarimeter of the Landessternwarte Heidelberg, Germany. This instrument consists of a focal reducer with a fixed polarisation sheet analyser behind a rotating achromatic $\lambda/2$–plate and uses a 22μ pixel-size GEC chip with 576 x 386 elements. A main characteristic of the polarimeter is the use of a focal reducer. With a reduction factor of 3.43, we obtain a large field of view (14.′4 x 9.′6) on the 1.23m Calar Alto telescope (aperture ratio f/8). This large field is required for the calibration of the different exposures, especially for the flux, seeing and background calibration. We lose angular resolution by the focal reducer, but the possible linear scale (in pc/pixel) does not change since we are able to observe appropriate nearby galaxies. However, the large field of view causes a relatively strong differential refraction which can rise up to typical values of about 0.1 pixel per 15′ over the whole series of observations. This will increase the calibration errors. The spectral range of the polarimeter is limited by the polarisation sheet analyser and the $\lambda/2$–plate to 400 - 750 nm (Huber 1989).

In the Appendix we briefly discuss the main characteristics of the instrument and the measurement principles. For further details see Huber (1989, 1990). Some important (non-standard) steps of the data reduction procedure are also discussed in the Appendix.

[1] The DSAZ is operated by the Max-Planck-Institut für Astronomie, Heidelberg, jointly with the Spanish National Commission for Astronomy.

3. Results and discussion

The results for each galaxy are shown in two different maps. One map shows the distribution of the polarisation vector superimposed on isocontours of the mean (of 16 frames) intensity, while the other map shows isocontours of the polarised intensity in an enlarged sub-image. All polarisation (E-)vectors with $0.05\% \leqq P \leqq 5\%$, $\Delta P \leqq 0.3P$, i.e. $\Delta\Theta \leqq 17°$, are plotted. The results of calibration measurements of the polarisation angle with standard stars are given in the Appendix.

Before discussing our results in detail, we will recall some typical features of polarisation in edge-on galaxies. In interstellar magnetic fields of the order of several μG strength the DGM may produce optical polarisation typically up to $\simeq 5\%$ with the orientation of the polarisation (E-)vectors parallel to the field. Thus a toroidal field in an inclined disk would produce polarisation parallel to the major axis, as seen e.g. in M 104 (Scarrott et al. 1990). However, anisotropic scattering of light from bright regions above the disk into the dust lane towards the line of sight may produce a similar pattern.

The scattering model of Jura (1982) demonstrated that polarisation of the order of 5%, with E-vectors parallel to the dark lane, may be produced. This result depends on the contribution of the stellar bulge to the light distribution. He recommended observations of optical polarisation in edge-on Sc galaxies as a test for the model.

On the other hand, Matsumara & Seki (1989) applied a 3D model and showed that light scattering by dust in a spheroidal galaxy (like M 104) would produce a polarisation pattern perpendicular to the major axis towards the centre. Although in the outer regions it is almost circular.

However, the two arguments, first that in the case of anisotropic scattering the interstellar dust, with a grain size comparable to optical wavelengths, is strongly forward-scattering and second that the polarisation vanishes for small scattering angles, imply a counterbalance between the polarisation efficiency and the scattering efficiency, which might hinder the detection of scattered polarised light.

In general, scattering is able to produce a higher amount of polarisation than the DGM, depending on the scattering angle. Assuming single scattering, the orientation of the polarisation

© European Southern Observatory • Provided by the NASA Astrophysics Data System

1996A&A...308..713F

vector is perpendicular to the scattering plane. A prominent example is M 82 with polarisation in Hα up to 40% in a circular pattern around the nucleus due to scattering in an extended dust halo (Bingham et al. 1976; Scarrott et al. 1991).

Whether the DGM or anisotropic scattering is the dominant mechanism, has to follow from a detailed discussion of both the degree of polarisation and the angular distribution. Measurements in different wavelengths may provide a direct criterion, since the DGM follows the Serkowski law while anisotropic scattering (Mie scattering) $\sim \lambda^{-1}$. Unfortunately, the optical spectral range seems to be too narrow to allow for a decisive fit to the Serkowski law. Scarrott et al. (1990) first measured the wavelength dependency of the polarisation in the dust lane of M 104. Those data fit the Serkowski law, but we note that $\sim \lambda^{-1}$ also gives a reasonable fit.

In general, the observed degree of polarisation in all three galaxies is in the range of the DGM. Therefore, both the DGM and anisotropic scattering effects have to be considered.

We know from radio observations (Dumke et al. 1995) that all three galaxies contain magnetic fields. We also know that these disk galaxies rotate differentially which provides the necessary condition for dynamo action. Especially, an $\alpha - \Omega$ dynamo is able to sustain the observed field strengths of a few μG by amplifying the toroidal field via differential shear (Ruzmaikin et al. 1988; Elstner et al. 1992; Brandenburg et al. 1993). Thus, one would expect to detect mainly toroidal (disk-parallel) fields. Radio polarisation measurements of most of the face-on galaxies observed indeed provide clear evidence for toroidal fields in those galaxies (e.g. Beck 1993).

Even though each of these galaxies considered here show differential rotation of the disk, providing the possibility of an α–Ω dynamo, we find in our data little indication for toroidal magnetic fields via the DGM. The dominant orientation of polarisation vectors are **perpendicular** to the major axis in all three galaxies despite their different positions on sky, their different intrinsic orientations, and even their different locations on the detector.

3.1. NGC 891

Fig. 1 shows the polarisation and the polarised intensity of NGC 891. It can be seen that the most prominent polarisation pattern is located to the south on both sides of the major axis (P.A. of the major axis $\simeq 65°$) at distances $\geq 1'$ from the obscured centre of the galaxy. The dominant orientation of the polarisation vectors are circular with respect to the centre. The degree of polarisation is between the range of 1% - 4% and rises with distance from plane. Whereas this region is characterised by a strongly obscuring dust lane, most of the polarisation does not appear in that lane but above and below that lane.

Another polarisation feature lies on the line of sight towards the obscured innermost central part of the galaxy. The degree of polarisation is $\lesssim 2\%$ and the polarisation angle on sky is $\simeq 140°$ or $\simeq 120°$ with respect to the major axis.

Note that even the total foreground polarisation, which has been mostly eliminated when calibrating the flux in our images by foreground stars, is weak ($P \leq 0.5\%$, $\Theta \simeq 100°$, see Mathewson & Ford 1970) compared to the polarisation measured in NGC 891.

Radio observations clearly prove the existence of a large-scale magnetic field in NGC 891. A flat spectral index in the plane ($\alpha \sim -0.4$, where $S \propto \nu^{\alpha}$) indicates enhanced production of relativistic electrons, e.g. by supernova explosions (Sukumar & Allen 1991; Hummel et al. 1991). This activity may drive a poloidal magnetic field (Lesch et al. 1989) or a galactic mass flow into the halo ("galactic wind"). As this galaxy rotates differentially, the action of a dynamo is exceedingly likely which preferably generates toroidal fields which are disk-parallel as long as the galactic wind is not too strong (Elstner et al. 1992; Brandenburg et al. 1993).

However, toroidal magnetic fields in NGC 891 can hardly be derived from our data since (a) we have observed polarisation predominantly perpendicular to the disk and (b) we did not detect polarisation in the dust lane.

The polarisation towards the centre of NGC 891 is mainly perpendicular to the disk and cannot be explained by single anisotropic scattering. Hence, we may have found evidence for a poloidal magnetic field towards the centre of the galaxy. Where this feature is located along the line of sight remains an open question. It is plausible that it is located in the outer (nearer) region of the galactic disk because of the strong absorption by the dust lane. Such "chimney-like" features also exist in the disk of the Milky Way and are most probably related to localised underlying star-formation activity (Müller et al. 1987). NGC 891 is well-known to host such chimney-like structures in the disk (Sofue 1987; Dettmar 1990).

In the outer parts of the galactic disk the polarisation is probably caused by anisotropic scattering of light from the bright central regime at high altitudes above the disk. This scenario would be similar to that of M82. The relatively low degree of polarisation could be explained by several effects. First, the light from the central part is obscured along the line of sight, it must also be obscured in direction of the outer scattering regions. Therefore, the fraction of scattered light from this region is small compared to the intrinsic light emission. Second, multiple scattering along the line of sight may decrease the degree of polarisation. Since the length scale of integration along the line of sight will decrease with distance along the major axis, the degree of polarisation will increase in the outer parts of the projected disk. This seems to be consistent with our observations.

If we compare the optical polarisation in the outer parts of the galaxy to radio data, we see that there are regions in the southern part of the galaxy where the optical polarisation vectors are aligned with the magnetic field as derived from radio observations (Hummel et al. 1991; Sukumar & Allen 1991). However, the global structure of the optical and radio data is quite different, suggesting that these observations correspond to two components of the galaxy which are intrinsically decoupled, i.e. dust (anisotropic scattering in the optical domain) and magnetic field (radio synchrotron emission), rather than the DGM of dust grains in the same magnetic field, which is respon-

© European Southern Observatory • Provided by the NASA Astrophysics Data System

1996A&A...308..713F

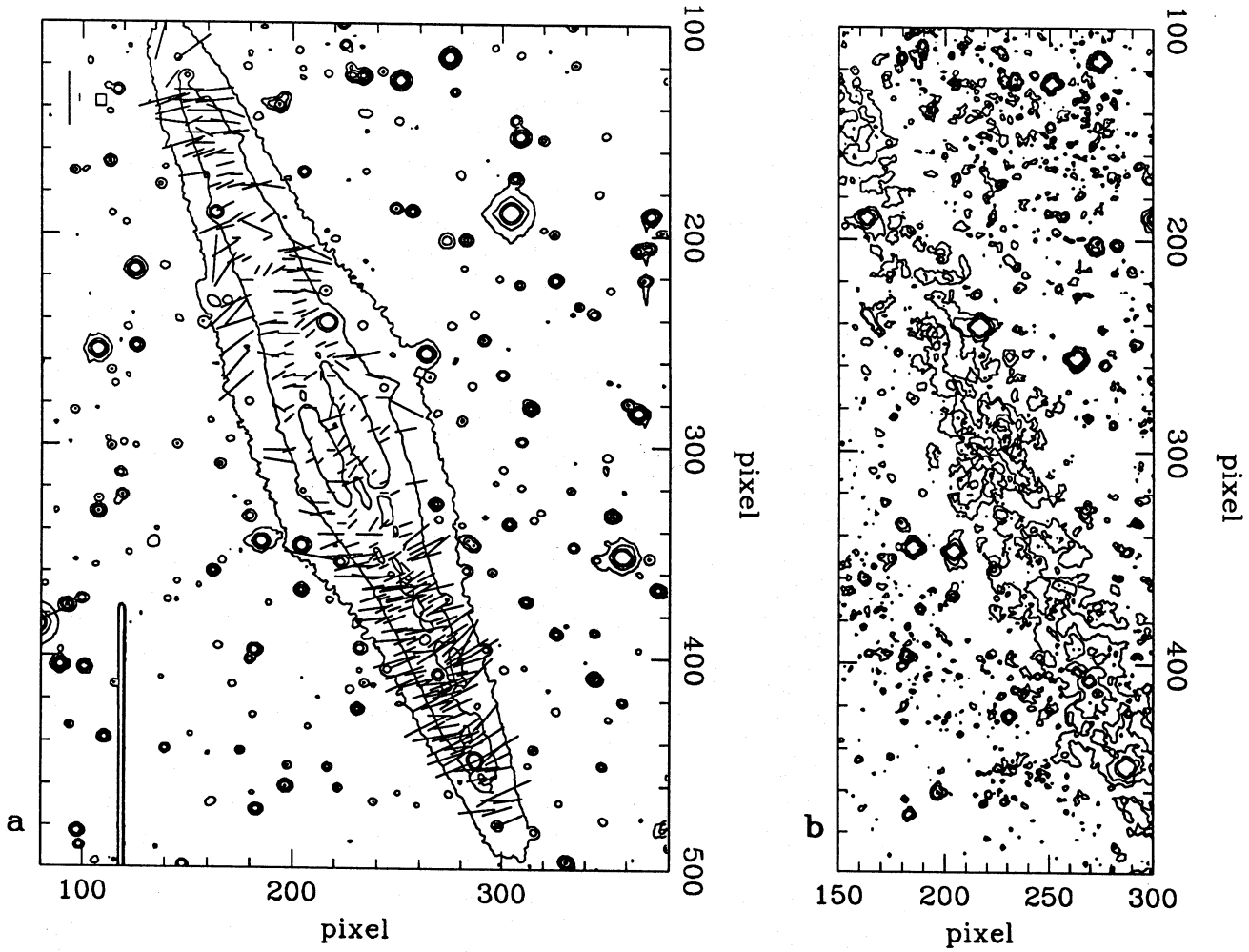

Fig. 1a and b. Linear optical polarisation of NGC 891. **a** Polarisation (E-)vectors superimposed by mean intensity contours. The polarisation degree is indicated by the length of the vectors, normalised to the vectors in the upper left corner of the frame (0.005 - 0.05). The polarisation degree is averaged over 5 x 5 pixel (see box in the upper left corner). Contour levels: 3.5^n ADU (linear instrumental unit, see Appendix), $n = 2, 3, 4, 5$. **b** Polarised intensity. Subset of the original frame, contour levels: 0.8, 2, 6 ADU

sible for the polarised radio emission. This idea receives further support from the distribution of the optically polarised intensity, where the lumpy structures are somewhat complementary to the contours of the polarised radio emission.

In the almost face-on spiral galaxy M51, the polarisation vectors in the optical range and the magnetic field vectors in the radio range are partly aligned, but deviate by up to 60° in some regions (Beck et al. 1987). Again a mixture of anisotropic scattering and DGM could explain this result.

The scale height of the gas distribution of about $\gtrsim 5$ kpc (Rand et al. 1990; Dettmar 1990) is similar to that of our polarisation pattern and widely exceeds the scale height for the dust distribution of $\simeq 0.22$ kpc (Kylafis & Bahcall 1987). This may indicate that we observe anisotropic scattering in the Rayleigh limit.

3.2. NGC 5907

Fig. 2 shows our results for NGC 5907. The polarisation pattern in a 2′ frame around the centre practically coincides with the result from Scarrott et al. (1990): The orientation of the polarisation vectors in this region is predominantly perpendicular to the disk with degrees of $\lesssim 1.5\%$. This pattern continues in the outer disk, while the degree of polarisation increases up to $\lesssim 4\%$. The outermost northern side shows more polarisation than the southern side.

An interesting feature is seen in the plot of the polarised intensity: The central single mean-intensity peak appears as a multiple source in polarised intensity. Furthermore, the contours in polarised intensity are more narrow than the mean-intensity contours and show more substructure. This substructure is more extended perpendicular to the disk in the eastern part of the galaxy.

Like NGC 891, the rotational velocities of NGC 5907 (Sancisi & van Albada 1987) suggest possible dynamo effects and

© European Southern Observatory • Provided by the NASA Astrophysics Data System

1996A&A...308..713F

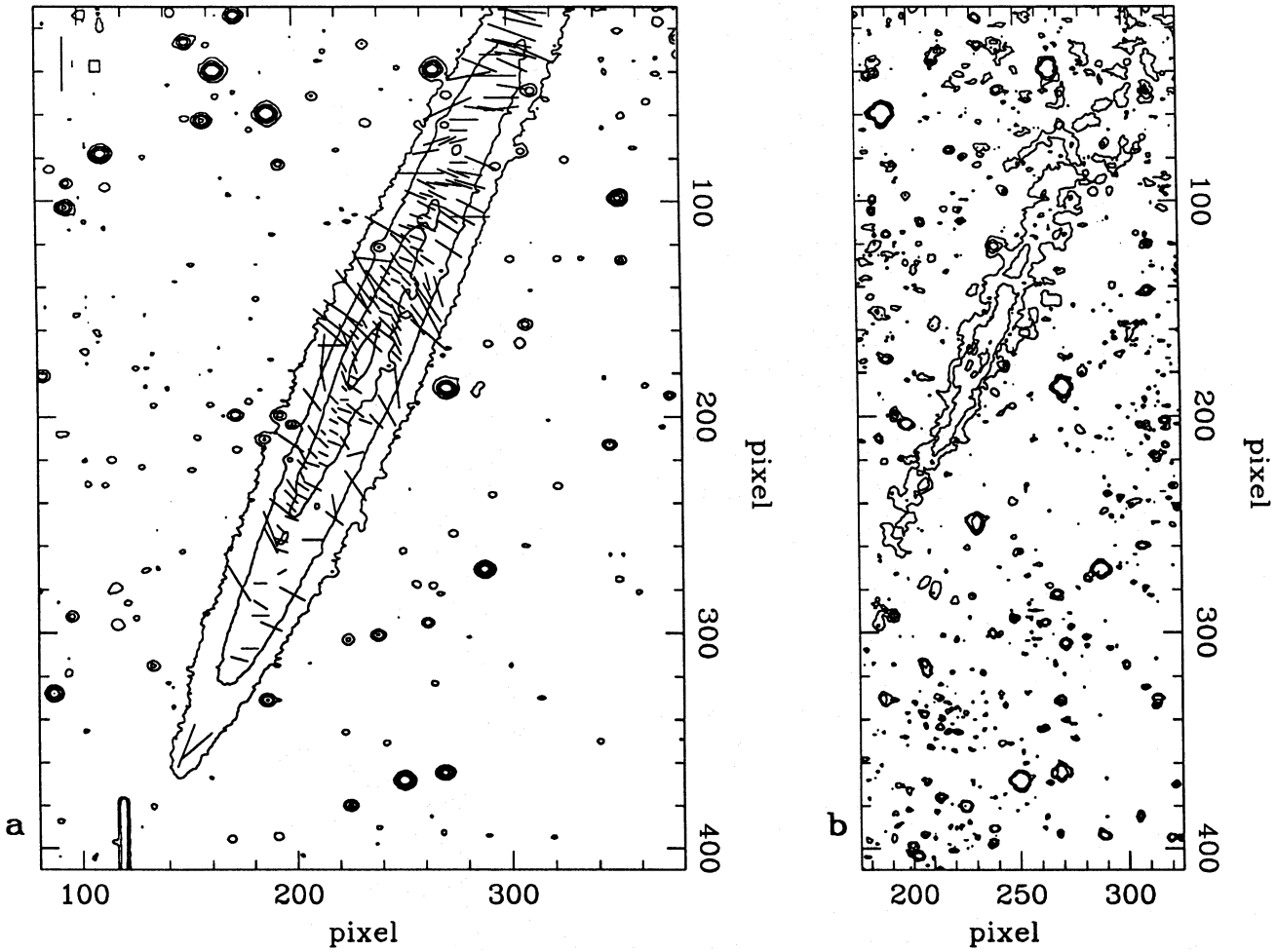

Fig. 2a and b. Linear optical polarisation of NGC 5907. **a** Text as in Fig. 1a. **b** Text as in Fig. 1b, but contour levels: 1.5, 3, 8 ADU

hence toroidal magnetic fields. The relatively steep radio spectral index $\alpha = -1.2$ (Hummel et al. 1984) shows that NGC 5907 is less active. Large-scale uniform magnetic fields are too weak to be detected (Dumke et al. 1995).

In a predominantly toroidal magnetic field, the DGM would produce a polarisation pattern parallel to the disk, in contrast to our observations. Scarrott et al. (1990) suggested that if the polarisation pattern perpendicular to the disk results from selective extinction, then, due to the inclination (86°) of the galaxy, the vertical component of the planar field is detected. However, since the inclination of NGC 5907 is very large, the parallel component of the toroidal magnetic field will always dominate the projected vertical field (at least by a factor $\cos^{-1} 86°$). From scattering models, Jura (1982) predicted that the polarisation of Sc galaxies may show E-vectors perpendicular to the disk along the major axis.

Thus, from our data, it seems plausible that anisotropic scattering causes the optical polarisation in NGC 5907. Similarly to NGC 891, we argue that the increase of the polarisation degree with distance along the major axis supports the anisotropic scattering scenario.

3.3. NGC 7331

Fig. 3 shows the optical polarisation of NGC 7331. The dominant polarisation pattern is located along the major axis, even far from the nucleus. In the polarised intensity map, the contours are reduced to a narrow streak; a pattern which is quite different from the elliptical contours of the mean intensity.

The degree of polarisation rises with distance from the centre. Particularly, in the southern-end region where dark dust clouds are visible on photographs (e.g. Sofue 1987), the polarisation increases to 5% and more. In the central part, the degree of polarisation is $\simeq$ 1%; a value which is close to the results of King (1986) and in contrast to of those of Elvius (1956).

In the dark lanes west of the nucleus, the observed polarisation pattern is parallel to the dust lanes. In the eastern part of the galaxy ($\simeq 1°$ from the nucleus), the polarisation is perpendicular to the major axis. For the innermost central part (10″ around the nucleus), Elvius (1956) found a similar orientation of the polarisation. Our large-field map shows that this pattern continues along the entire minor axis.

In the inner part of the galaxy, our result is similar to that of King (1986). In particular, along the major axis, the orientation

© European Southern Observatory • Provided by the NASA Astrophysics Data System

1996A&A...308..713F

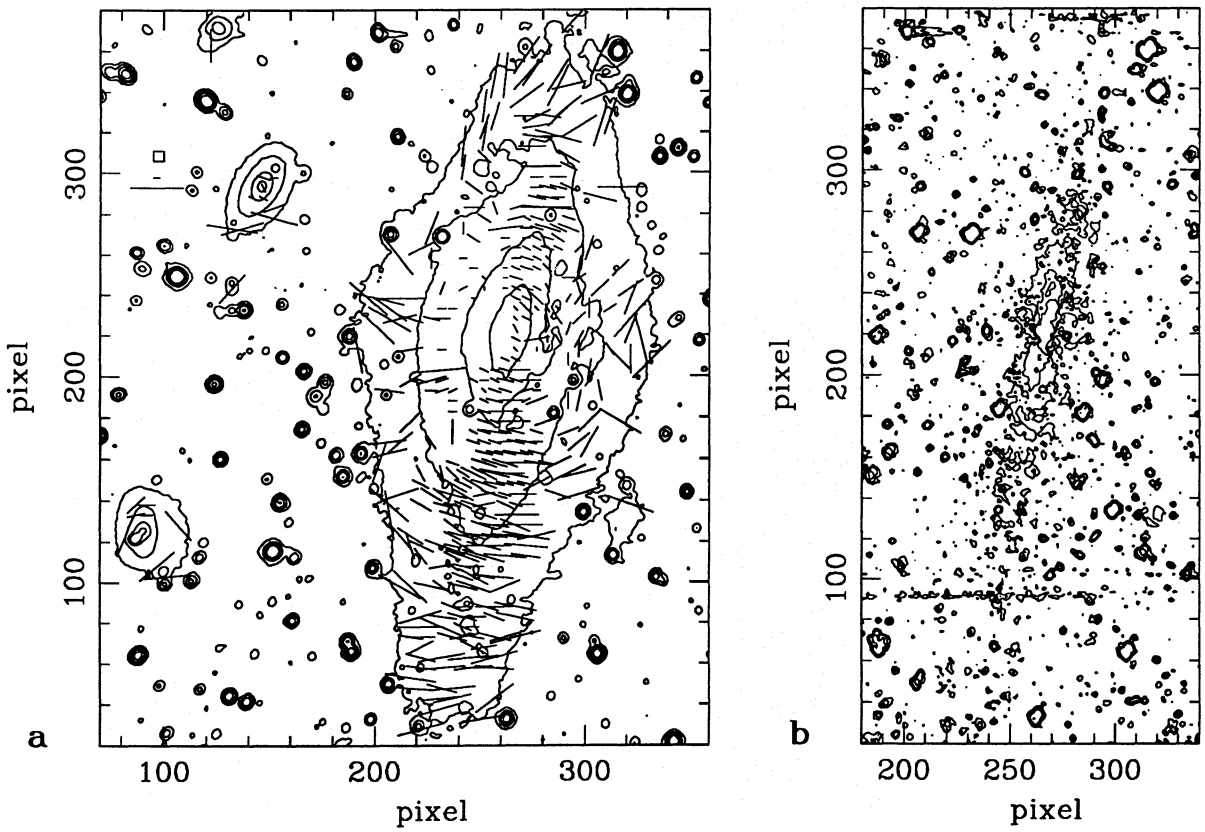

Fig. 3a and b. Linear optical polarisation of NGC 7331. Text as in Fig. 1

of the polarisation vectors is the same and the lack of polarisation north-east and south-west from the nucleus is also similar to King. In contrast to King and Elvius we detected no polarisation east of the nucleus.

The centre of the galaxy, as well as the centre of the small companion in the north-east show similar polarisation vectors of $P \simeq 1\%, \Theta \simeq 30°$. This signature may be interpreted as a relict of foreground polarisation. However, as argued in the Appendix, our polarisation map should be adequately corrected for foreground polarisation. The central polarisation feature in the main galaxy could, however, be explained by an error in the offset reduction, since the nucleus is very bright and has a very steep intensity profile. This may happen because a small error in the flux conservation of the pixel intensities during the rebinning procedure results in an artificial flux variation at the pixel position and, hence, would produce a pseudo polarisation. However, this effect would only influence the results in the high intensity central pixels with a steep intensity profile.

NGC 7331 contains a large-scale magnetic field which is closely related to the spiral structure (Dumke et al. 1995). Galactic activity and therefore poloidal magnetic fields could be inferred from the galactic nucleus as a LINER (Low Ionisation Narrow Emission-line Region) and the detection of a molecular cloud ring (Young & Scoville 1982) which is statistically related to activity (Arsenault 1989). However, radio observations at high frequencies do not reveal an indication of a poloidal magnetic field (Dumke et al. 1995).

As already suggested by King (1986), the very bright nucleus provides an excellent scattering source. While discussing possible scattering effects, in NGC 7331 one has to keep in mind that the galaxy is not seen fully edge–on but with an inclination of 70°. This implies that all of the scattered light may be detected, since the dusty disk does not lie along the line of sight, as is the case for NGC 891 and 5907. Isotropic scattering of light from the central source along a tilted disk would then lead to a quasi-circular (or elliptic) orientation of the polarisation pattern. However, interstellar dust is known to be strongly forward–scattering and, assuming this anisotropic scattering scenario, the resulting polarisation would have an asymmetric pattern. The western (closer) side of the galaxy shows a higher degree of polarisation than the more distant eastern side. The latter argument been discussed up by King (1986).

Our results show indeed more polarisation at the western than the eastern side. Also note that the western side shows strong dust lanes while the eastern side does not and that forward–scattering has a very low polarisation efficiency. Thus, an active DGM in the western dust lanes can not be excluded. In fact, since the polarisation pattern in the western part follows more the linear extended dust lane over $\simeq 3'$ rather than a circular pattern, we believe that here the polarisation is due to the DGM. This is also supported by the fact that light from the nucleus would be obscured by the dust disk in direction to the dust lane. A further argument in favour of the DGM comes from

© European Southern Observatory • Provided by the NASA Astrophysics Data System

1996A&A...308..713F

the observation that the polarisation vectors in the dust lane are not *very* well aligned as one would expect from scattering.

What causes the polarisation at the eastern side remains unclear. Scattering effects seem to be unrealistic because of the polarisation angle of 90° towards the major axis and the vanishing polarisation efficiency for small scattering angles. A DGM operating in the galactic disk with a toroidal magnetic field would give a different polarisation pattern. Vertical magnetic fields, theoretically proposed for active galaxies (Lesch et al. 1989) and, also, observed for other galaxies (e.g. NGC 891), together with an additional mass outflow, which was observed for NGC 1808 (Scarrott et al. 1993), may provide an explanation. If this is true, from the de-projection of the galaxy and the polarisation pattern, we can estimate the scale height of the hypothetical vertical field and wind outflow to be of the order of 0.5′ or 3 kpc.

The appearance of strongly enhanced polarisation along the major axis could be explained by the expected scattering angles of $\simeq 90°$, which imply a high degree of polarisation (see also King 1986). Besides the major axis, the scattering angles increase (decrease) at the near (far) side of the galaxy and, therefore, the polarisation decreases. Along the minor axis, the scattering angles are 160° and 20°, respectively. The ratio of polarisation degree between the major and minor axis, derived solely from these geometrical aspects, would be of the order of $\lesssim 10$.

Further indication for an active DGM can be found in the far south of the galaxy, where the strong polarisation coincides with a dark dust cloud region and the orientation seem to follow the spiral arm. In these regions, the bright nucleus may also be obscured by the dust disk, but here, the optical depth towards the observer is small enough to allow a detection of the DGM.

4. Summary

In this paper we presented large-scale linear optical polarisation maps of the spiral galaxies NGC 891, 5907 and 7331.

In the case of NGC 891 our results indicate that most of the observed polarisation comes from anisotropic scattering. No evidence for toroidal magnetic fields was found, but this result may be limited by the observational noise achieved. However, towards the centre of NGC 891 we found evidence for the Davis-Greenstein mechanism (DGM).

The polarisation of NGC 5907 is orientated perpendicular to the disk at all locations. In the inner part our results agree with those of Scarrott et al. (1990). As high-frequency radio polarisation measurements show no strong poloidal magnetic fields (Dumke et al. 1995), we conclude that anisotropic scattering is the dominating effect.

In NGC 7331 the overall polarisation pattern seems to be dominated by scattering of light from the bright nucleus along the major axis. We found observational evidence for toroidal magnetic fields only along the western dust lane which is confirmed by high-frequency radio polarisation observations (Dumke et al. 1995).

A promising future prospect concerning the detection of magnetic fields in galaxies is provided by far-infrared and sub-mm observations (Hildebrand 1988, Hildebrand & Davidson 1994). In these spectral regimes, anisotropic scattering effects are less important, and, hence, the DGM may observed directly.

Acknowledgements. We like to thank R. Östreicher and I. Appenzeller for many instructive comments on the properties of optical polarisation and magnetic fields in galaxies. We are grateful to R. Wielebinski and I. Appenzeller for their continuous support for this project. The Max-Planck-Gesellschaft is acknowledged for financial support of the project, and the staff of the DSAZ for help during the observations. We appreciate the work done by C. Hartlieb and the mechanical workshop of the Landessternwarte in building and maintenance of the focal reducer polarimeter.

Appendix A: instrument and observations

A.1. The instrument

The polarisation optics consists of a fixed polarisation sheet analyser behind a rotating achromatic $\lambda/2$–plate. Both are located near the focal plane of the telescope in front of the optical system of the focal reducer. Rotation of the $\lambda/2$–plate by an angle Φ_i turns the **E**-vector of the linearly polarised part of the incoming light by an angle of $2\Phi_i$ while the underlying sheet analyser remains fixed. A full rotation of the $\lambda/2$–plate in steps of 22.°5 imply a set of 16 exposures at 16 different positions.

In contrary to polarimetry techniques working with splitting the incoming light in two beams polarised perpendicular to each other (e.g. Scarrott et al. 1983), we get a complete image of the object in every position of the $\lambda/2$–plate. On the other hand, light polarised perpendicular to the axis of the sheet analyser, i.e. half of the incoming light, will not be detected.

A.2. Principle of measurement

The normalised ideal signal $S_N(\Phi_i)$ measured on the detector varies with the position Φ_i of the $\lambda/2$–plate as

$$S_N(\Phi_i) = 1 + P_x \cos(4\Phi_i) + P_y \sin(4\Phi_i)\,, \tag{A1}$$

with the normalised Stokes parameters $P_x = P\cos(2\Theta)$ and $P_y = P\sin(2\Theta)$. P and Θ denote the degree of polarisation and the polarisation angle, respectively. Using Fourier analysis, the polarisation follows from the $4\Phi_i$ Fourier components

$$P_x = \frac{1}{8}\sum_{i=1}^{16} S_N(\Phi_i)\cos(4\Phi_i)\,, \tag{A2}$$

$$P_y = \frac{1}{8}\sum_{i=1}^{16} S_N(\Phi_i)\sin(4\Phi_i)\,, \tag{A3}$$

$$P = \sqrt{P_x^2 + P_y^2}\,, \quad \Theta = \frac{1}{2}\arctan\frac{P_y}{P_x} + \frac{m\pi}{2}\,, \tag{A4}$$

where m controls the orientation of the polarisation vector with respect to the P_x–P_y space,

$$m = 0 \;\forall\; P_x > 0, P_y > 0\,,$$

© European Southern Observatory • Provided by the NASA Astrophysics Data System

1996A&A...308..713F

$$m = 2 \;\forall\; P_x > 0, P_y < 0\,,$$
$$m = 1 \;\forall\; P_x < 0\,. \tag{A5}$$

A.3. Calculation of the error

Equation (A1) holds for an ideal signal. Practically, intensity modulations of other Fourier frequencies add to the $4\Phi_i$ signal. Therefore, the real modulation is a superposition of a certain number of possible Fourier components limited by the sampling theorem: N measurements allow for the calculation of $N/2$ Fourier components, leading to a signal

$$S_N(\Phi_i) = 1 + \sum_{n=1}^{N/2} P_x^n \cos(n\Phi_i) + P_y^n \sin(n\Phi_i)\,. \tag{A6}$$

The additional Fourier components are caused by different effects:

1. 1Φ : Dirt or dust on the $\lambda/2$–plate, white noise.
2. 2Φ : Pleochroism of the $\lambda/2$–plate, white noise, harmonic of the 1Φ–component.
3. 4Φ : Polarisation, white noise, harmonics.
4. $3, 5 - 8\Phi$: White noise, harmonics.

As a measure for the error in the degree of polarisation ΔP, we take the mean of the amplitudes P_x^n, P_y^n of the additional Fourier components

$$P_x^n = \frac{1}{8}\sum_{i=1}^{16} S_N(\Phi_i)\cos(n\Phi_i)\,, \tag{A7}$$

$$P_y^n = \frac{1}{8}\sum_{i=1}^{16} S_N(\Phi_i)\sin(n\Phi_i)\,, \tag{A8}$$

$$\Delta P = \frac{1}{5}\left(\sqrt{(P_x^3)^2 + (P_y^3)^2} + \sum_{n=5}^{8}\sqrt{(P_x^n)^2 + (P_y^n)^2}\right). \tag{A9}$$

Thus, ΔP measures the mean amplitude of the Fourier components caused by white noise and harmonics.

With Eq. (A9), the error in the polarisation angle $\Delta\Theta$ can be approximated by

$$\Delta\Theta = \frac{1}{2}\arctan\frac{\Delta P}{P} \tag{A10}$$

which becomes plausible in a P_x–P_y diagram.

Fig. 4b shows the amplitudes of the 8 Fourier components $P^n = \sqrt{(P_x^n)^2 + (P_y^n)^2}$ for a small frame of 10 x 10 pixels in the region of the galaxy and the sky background, respectively. The increased amplitude of the 4Φ component in the galaxy indicates linear polarisation. From this, Eq. (A9), the calculation of the error as the mean amplitude of the $3, 5, 6, 7, 8\Phi$ components, becomes plausible.

Appendix B: data reduction

The signal S_{ij}^n, measured by each pixel (i, j) or (l, m) and position (n) of the $\lambda/2$–plate, can be represented as

$$S_{ij}^n = B_{ij} + D_{ij} + f_{ij}\cdot L_{ijlm}^n(s^n \otimes (F^n \cdot (H_{lm}^n + O_{lm}^n)))\,, \tag{B1}$$

where the additive and multiplicative terms are the bias B, the dark current D, the intrinsic intensity of the galaxy O, and the sky background H. The flat field function f describes the illumination and the sensitivity of the CCD detector, the matrix L corresponds to the frame offset between each exposure, the function F measures the relative flux of each exposure. Each exposure has to be convolved with the seeing function s, depending on the seeing conditions.

Thus, the procedure of data reduction is as follows: After the usual standard reduction (subtraction of the bias, dark current, and the sky background; flat fielding) for each frame separately, additional steps are required in order to combine all 16 frames together. These are:

1. Convolution to the same (worst) seeing.
2. Linear offset reduction (rebinning).
3. (Relative) flux calibration.

Finally, Fourier analysis provides the polarisation images, i.e. P, ΔP, Θ for each pixel. In addition, we have to correct for the instrumental polarisation offset angle. This could be done using standard stars (see below) and/or laboratory measurements.

In the following, we discuss the reduction steps applied for the combination of the 16 frames more detailed, since they may cause systematic errors in addition to the statistical error.

B.1. Seeing calibration

Intensity modulations due to seeing variations between the 16 exposures would cause a pseudo polarisation, depending on the scale of the seeing variation as well as on the intensity profile. For each frame we calculate a mean seeing σ^n, using Gaussian fits of a set of field stars. Then the frame is convolved to the worst seeing σ_{max}, using

$$(\sigma^n)_\Delta^2 = (\sigma_{max})^2 - (\sigma^n)^2. \tag{B2}$$

Numerical problems in the Gaussian fit due to intensity undersampling for some field stars affect the seeing calibration. Such stars have to be excluded from the seeing reduction.

B.2. Flux calibration

Variations in transparency between the single exposures and sometimes different exposure times are causing intensity modulations which are not due to polarisation. In order to eliminate these effects, we calibrate the intensity flux of the galaxy in each frame to the mean flux of foreground stars.

In principle, the foreground polarisation of the Galaxy is automatically reduced by this procedure, but, practically, there is a limit: A good signal-to-noise ratio requires bright stars for

© European Southern Observatory • Provided by the NASA Astrophysics Data System

1996A&A...308..713F

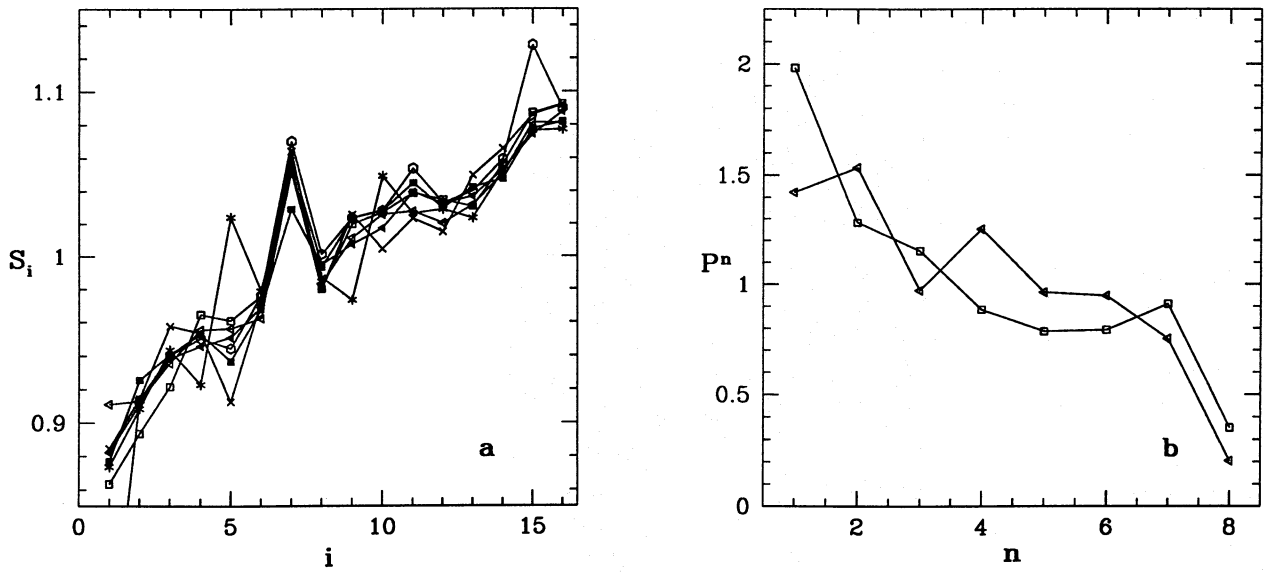

Fig. 4. a Variation of the normalised flux S_i, (i = 1...16) of a sample of field stars around NGC 891 during the 16 exposures. **b** Amplitudes of the Fourier components P^n, (n = 1...8) for a certain region in the galaxy NGC 891 (◁) and the sky background (□), respectively

the flux calibration, i.e. mainly nearby stars, while for the elimination of the foreground polarisation the most distant field stars, i.e. the faint stars, are more appropriate for the calibration. Furthermore, if field stars from different distances (and, thus, with a different amount of foreground polarisation) are used for the flux calibration, the foreground polarisation could not absolutely be reduced.

The calibration stars have to be selected very carefully. Stars with a 'strange' variation, e.g. due to cosmic events, the influence of dust on the $\lambda/2$–plate, and even unknown reasons, were neglected for the flux calibration (see Fig. 4a). Typically ≈20 stars with a 'good', i.e. similar behaviour can be found over the set of frames. The summarised intensity of about 700000 ADU (linear instrumental unit; conversion factor 16 electrons per ADU) corresponds to a statistical error $\Delta P \approx 0.03\%$ due to white noise.

If only very few field stars are available for the flux calibration, it is preferable to calibrate using $\sqrt{S}$, instead of the intensity S as a measure for the flux (which is possible, since we are dealing with a *relative* flux calibration). This would reduce the erratic influence of hypothetical, irregular flux variations of a dominating, bright star.

Fig. 4a shows the flux variation of a sample of field stars in the frame of NGC 891 during the set of 16 exposures. It can be clearly seen that the galaxy is *rising* in the sky. Improved atmospheric conditions are indicated during rotational step n = 7. Some stars show a strange behaviour compared to the overall variations and therefore have to be excluded from the flux calibration of the galaxy. No clear 4Φ periodicity of the field stars (indicating polarisation) is visible.

Table 1. Instrumental angular offset calibration using polarised standard stars (Bastien et al. 1988, Dolan & Tapia 1986). Measurements with our instrument (obs) and the value given by the literature (lit) are shown.

Star	Source	P	ΔP	Θ	$\Delta\Theta$
HD 204827	obs	4.68	0.80	7.59	4.9
	lit	5.70	0.03	59.3	0.1
HD 154445	obs	2.2	1.6	36.2	18.0
	lit	3.73	0.01	90.1	0.1
HD 183143	obs	5.09	0.24	130.9	1.3
	lit	6.08	0.05	179.3	0.2
HD 161056	obs	3.52	0.41	15.8	6.5
	lit	4.08	0.07	69.0	0.2

B.3. Instrumental offset angle

Table 1 shows the results of measurements of polarised standard stars. This is necessary for the reduction of the offset angle between the the instrumental polarisation angle and the northern orientation on sky.

The measurement principle is similar to the procedure for the galaxy exposures. However, instead of reading out the whole CCD frame, only a 50 x 50 pixel field around the star and a corresponding background field is applied. Due to the fast readout time we were able to observe all 16 frames within one minute. Thus, variations in transparency and seeing could be neglected for the data reduction of the standard stars and it is possible to get an online information on the offset angle.

We finally derived an instrumental offset angle against the south-north meridian on sky of $48\overset{\circ}{.}9 \pm 1\overset{\circ}{.}9$. This was calculated from the mean deviation between the observed polarisation angle and the literature value of the the polarisation angle.

© European Southern Observatory • Provided by the NASA Astrophysics Data System

1996A&A...308..713F

B.4. Foreground polarisation of NGC 7331

As mentioned in Sect. B.2, the foreground polarisation should be automatically reduced by the relative flux calibration via foreground stars. However, a weak residual polarisation towards the very centre of NGC 7331 was found (see Fig. 3a). The following arguments suggest that this is not an effect of the foreground polarisation:

1. The field stars show no polarisation, except single examples with a high intensity gradient profile where the polarisation ($P \simeq 30\%$) at the wings of the intensity profile follows from spatial offset reduction errors or from the seeing reduction.
2. From the polarisation map of Mathewson & Ford (1970) we estimate the foreground polarisation to $P \simeq 0.5\%, \Theta \simeq 80°$ which is nearly consistent with the result of King (1986), who measured a central polarisation of NGC 7331 of $P = 0.8\% \pm 0.3\%, \Theta = 78° \pm 16°$ and a foreground polarisation of $P = 0.7\% \pm 0.2\%, \Theta = 51° \pm 32°$, derived from six bright foreground stars. Despite from the fact that bright stars may not exhibit the whole foreground polarisation along the line of sight to the galaxy (Sect. 3.2), it is not possible to reduce our central polarisation pattern with the preceding estimates.

References

Appenzeller I., 1967, PASP 79, 600
Arsenault R., 1989, A&A 217, 66
Bastien P., Drissen L., Menard F., Moffet A.F.J., Robert C., St-Louis N., 1988, AJ 95, 900
Beck R., 1991. In: Bloemen H. (ed.) Proc. IAU Symp. 144, The Interstellar Disk-Halo Connection. Kluwer, Dordrecht, p. 267
Beck R., 1993. In: Krause F., Rädler K.-H., Rüdiger G. (eds.) Proc. IAU Symp. 157, The Cosmic Dynamo. Kluwer, Dordrecht, p. 283
Beck R., Klein U., Wielebinski R., 1987, A&A 186, 95
Bingham R.G., McMullan D., Phallister W.S., White C., Axon D.J., Scarrott S.M., 1976, Nature 259, 463
Brandenburg A., Donner K.J., Moss D., Shukurov A., Sokoloff D.D., Tuominen I., 1993, A&A 271, 36
Davis L., Greenstein J.L., 1951, ApJ 114, 206
Dettmar R.-J., 1990, A&A 232, L15
Dolan J.F., Tapia S., 1986, PASP 98, 792
Dumke M., Krause M., Wielebinski R., Klein U., 1995, A&A (in press)
Elstner D., Meinel R., Beck R., 1992, A&AS 94, 587
Elvius A., 1956, Stockholms Observatoriums Annaler Band 19, No. 1, 3
Hall J.S., 1949, ApJ 54, 187
Hiltner W.A., 1949, Nature 169, 283
Hildebrand, R.H., 1988, Quart.J.R.astr.Soc., 29, 327
Hildebrand, R.H., Davidson, J.A., 1994. In: Genzel, R., Harris, A.I. (eds.), The Nuclei of Normal Galaxies. Kluwer, Dordrecht, p. 199
Hiltner W.A., 1949, Nature 169, 283
Huber A., 1989, *Diploma thesis*, University of Heidelberg
Huber A., 1990. In: Beck R., Kronberg P.P., Wielebinski R. (eds.) Proc. IAU Symp. 140, Galactic and Intergalactic Magnetic Fields. Kluwer, Dordrecht, p. 252
Hummel E., Sancisi R., Ekers R.D., 1984, A&A 133, 1
Hummel E., Beck R., Dahlem M., 1991, A&A 148, 23
Jura M., 1982, ApJ 258, 59
King D.J., 1986, MNRAS 220, 485
Kronberg P.P., 1994, Rep. Prog. Phys. 57, 325
Kylafis N.D., Bahcall J.N., 1987, ApJ 317, 637
Lesch H., Crusius A., Schlickeiser R., Wielebinski R., 1989, A&A 217, 217, 99
Mathewson D.C., Ford V.L., 1970, Mem. Roy. Astron. Soc. 74, 139
Matsumara M., Seki M., 1989, A&A 209, 8
Müller P., Reif K., Reich W., 1987, A&A 183, 327
Rand R.J., Kulkarni S.R., Hester J.J., 1990, ApJ 352, L1
Ruzmaikin A.A., Shukurov A.M., Sokoloff D.D., 1988, Magnetic Fields of Galaxies. Kluwer, Dordrecht
Sancisi R., van Albada T.S., 1987. In: Kormendy J., Knapp G.R. (eds.), Dark matter in the Universe. Kluwer, Dordrecht, p. 67
Scarrott S.M., Warren-Smith R.F., Phallister W.S, Axon D.J., Bingham R.G., 1983, MNRAS 204, 1163
Scarrott S.M., Rolph C.D., Semple D.P., 1990. In: Beck R., Kronberg P.P., Wielebinski R. (eds.) Proc. IAU Symp. 140, Galactic and Intergalactic Magnetic Fields. Kluwer, Dordrecht, p. 245
Scarrott S.M., Eaton N., Axon D.J., 1991, MNRAS 252, 12p
Scarrott S.M., Draper P.W., Stockdale D.P., Wolstencroft R.D., 1993, MNRAS 264, L7
Serkowski K., 1973. In: Greenberg J.M., van de Hulst H.C. (eds) Interstellar Dust and Related Topics. Reidel, Dordrecht, p. 145
Sofue Y., 1987, PASJ 39, 547
Spitzer, L., Jr., 1978, Physical Processes in the Interstellar Medium. Wiley, New York
Sukumar S., Allen R.J., 1991, ApJ 382, 100
Wainscot R.J., de Jong T., Wesselius P.R., 1987, A&A 181
Young J., Scoville N., 1982, ApJ 260, L41
Wielebinski R., Krause F., 1993, Astron. Astrophys. Rev. 4, 449

Note added in proof: After this paper was accepted, the work by Bianchi, Ferrara & Giovanardi came to our attention (In: W. Roberge and D. Whittet (eds.) Polarimetry of the Interstellar Medium, A.S.P. Conf. Ser., in press). The authors perform 3D MonteCarlo simulations of dust absorption and multiple scattering in spiral galaxy models. Their results show a polarisation pattern perpendicular to the major axis for nearly edge-on galaxies due to scattering and extinction effects, which is in agreement with our conclusions.

This article was processed by the author using Springer-Verlag LaTeX A&A style file version 3.

© European Southern Observatory • Provided by the NASA Astrophysics Data System